



Model for Transition from Waves to Synchrony in the Olfactory Lobe of Limax

BARD ERMENTROUT*

Department of Mathematics, University of Pittsburgh, Pittsburgh, PA 15260, USA

JING W. WANG

Division of Biological Sciences, University of California, San Diego, 2218 Bonner Hall 9500 Gilman Drive, La Jolla, CA 92093-0368, USA

JORGE FLORES

Center for Neurobiology and Behavior, Columbia University, New York, NY 10032, USA

ALAN GELPERIN

Monell Chemical Senses Center, 3500 Market St., Philadelphia, PA 19104, USA

Received March 19, 2004; Revised July 7, 2004; Accepted July 14, 2004

Action Editor: Christiane Linster

Abstract. A biophysical model for the interactions between bursting (B) cells and nonbursting (NB) cells in the procerebral lobe of *Limax* is developed and tested. Phase-sensitivity of the NB cells is exhibited due to the strong inhibition from the rhythmically bursting B cells. Electrical and chemical junctions coupled with a parameter gradient lead to sustained periodic waves in the lobe. Excitatory interactions between the NB cells, which rarely fire, lead to stimulus evoked synchrony in the lobe oscillations. A novel calcium current is suggested to explain the effects of nitric oxide (NO) on the lobe. Gap junctions are shown both experimentally and through simulations to be required for the oscillating field potentials.

Keywords: oscillations, waves, olfaction, limax, nitric oxide, gap junctions

1. Introduction

Information processing in the olfactory system typically involves oscillatory dynamics of ongoing or odor-elicited activity in early odor processing centers (Dorries and Kauer, 2000; Gelperin, 1999; Lam et al., 2000; Laurent et al., 2001; Martin et al., 2004). The computational role of oscillatory dynamics in olfaction is not yet known in detail, although two recent manipu-

lations of oscillatory dynamics during odor processing suggest a role for oscillations in discriminating between closely related odors (Stopfer et al., 1997; Teyke and Gelperin, 1999). Detailed knowledge as to how input from olfactory receptors affects the cooperative dynamics of mitral cells in olfactory bulb and mitral cell analogs in invertebrates would help clarify the computational role of oscillatory dynamics in olfaction.

The early olfactory system of the terrestrial mollusc *Limax maximus* is well suited to studies of oscillatory dynamics and olfactory information processing.

*To whom correspondence should be addressed.

The structure which receives direct olfactory input, the procerebral (PC) lobe of the cerebral ganglion, displays 0.7 Hz oscillations in local field potential (LFP) which are modulated by olfactory input (Gelperin and Tank, 1990; Gervais et al., 1996; Kimura et al., 1998c; Toda et al., 2000). The PC lobe also propagates activity waves from its apical to basal pole at 1.1 mm/sec in vitro (Delaney et al., 1994; Kimura et al., 1998b; Kleinfeld et al., 1994). The activity waves serve to separate odor representations set up in the PC lobe by associative conditioning when odors are used as conditioned stimuli (Ermentrout et al., 2001; Gelperin, 1999; Kimura et al., 1998a).

The traveling activity wave in the Limax PC lobe results from interactions among a group of bursting (B) neurons which have a gradient of excitability from apex to base of the PC lobe (Ermentrout et al., 1998). Figure 4A of this paper shows slices of the procerebral lobe from the apical region of the PC lobe oscillate at a higher frequency than slices taken from the basal region. This is interpreted to show that B neurons in the apical region are more excitable, i.e., have a higher frequency of bursting, than B neurons in the basal region. The B neurons are coupled local inhibitory neurons which produce 5–7 mV IPSPs in nonbursting (NB) neurons, first in the apical region and then in successively more basal NB cells as the activity wave propagates from apex to base in the B neuron network (Wang et al., 2001). The LFP arises mainly from the coherent postsynaptic currents in the local population of NB neurons elicited by coherent bursting in the local B cells (Watanabe et al., 1998, 1999, 2001).

At rest the PC lobe produces oscillatory waves. Either spontaneously or after odor input the PC can switch from waves to brief bouts of apical-basal synchrony. Odor inputs make afferent synapses onto excitatory interneurons, the NB cells. Shocking olfactory input fibers results in phase-dependent modulation of the LFP (Gelperin and Tank, 1990). This is a consequence of phase dependent activation of NB cells and their excitatory synapses onto B cells (Inoue et al., 2000). In addition to direct fast excitation from NB cells onto B cells, NB cell activity may induce the release of nitric oxide (NO) onto B cells, which causes an increase in B cell burst frequency and an increase in LFP frequency (Gelperin, 1994). In an earlier paper (Ermentrout et al., 1998) we used an abstract model of coupled phase oscillators to explain the origin of the phase lags of the LFP as well as the transient synchrony

due to odor inputs. In order to explain several recent experimental results, we now introduce simplified biophysical models for B and NB cells and couple them into networks. The coupled networks show waves, transient synchrony to inputs and phase-dependence of the long-lasting LFP frequency increase to inputs. Additionally, we describe several new physiological experiments and use the model to explain these. We show that uncaged NO can lead to a change in the frequency of the rhythm as well as a change in the direction of propagation and that this alteration is location dependent. We furthermore assess the role of electrical coupling in the PC lobe and its importance in maintaining both the rhythm and the structure of the wave.

2. Methods

2.1. Experimental

2.1.1. Distribution of Bursting Neurons. Anatomical studies of the number and distribution of burster neurons in the Limax PC lobe used desheathed PC lobes from newly hatched slugs incubated at room temperature for 20 min in slug saline containing 5 ng/ml sulforhodamine 101 (Molecular Probes) (Cina and Hochman, 2000) or 0.005% Hoechst 33258 (Sigma). The latter is normally used to stain nuclear DNA (Bale et al., 2001) but we found that Hoechst 33258 labels burster neurons with the same specificity as sulforhodamine 101 (Wang et al., 1999). Excess dye was removed by rinsing the PC lobe with saline containing 1% BSA for one hour. Stained neurons were visualized with a custom-built two-photon laser-scanning microscope (TPLSM) (Denk and Svoboda, 1997). The excitation wavelength was 830 nm. Image files from TPLSM were analyzed using NIH image v. 1.57. Some preparations were examined in 150 μ m thick vibratome sections made after embedding the desheathed PC lobe in low melting point agar.

2.1.2. Electrophysiology of the PC Lobe. The PC lobe was isolated by fine dissection after anesthetizing slugs (*Limax maximus*) by exposure to 5°C and injection of cold isotonic (55 mM) MgCl₂. Dissection of the CNS to isolate the PC lobe is done in high magnesium (5X) cold saline. After return to normal saline at room temperature the LFP oscillation and apical-basal wave propagation are very regular. Dual field potential

recordings from the PC lobe used saline-filled patch electrodes (3–5 μm tip) inserted into the cell body layer at the apex and base of the lobe. Field potential signals were recorded with HEKA EPC-7 amplifiers, digitized at 500 Hz and recorded on computer (Apple Mac II) using custom software. The olfactory nerve (ON) was severed at its peripheral origin in the digitate ganglion and placed in a tight fitting suction electrode for stimulation. The phase of the ON shock was calculated as the time from the LFP peak to the shock divided by the duration of the last complete LFP cycle prior to the shock. To measure the effects of gap junctional blockers such as 18 α glycyrrhetic acid (GA) (Bou-Flores and Berger, 2001; Davidson and Baumgarten, 1988; Wong et al., 1998) and octanol (OCT) (Mills and Massey, 2000; Spray et al., 1985) we recorded intracellularly from buccal cells B7 and SB (Copeland and Gelperin, 1983; Prior and Gelperin, 1977) and measured the decrease in their electrical coupling caused by addition of the gap junctional blocker. Effects of uncoupling agents and molluscan glutamatergic modifiers like picrotoxin (PTX) (Cleland, 1996) were assessed by dual recordings (apical and basal) of the LFP in the isolated PC lobe to measure the phase delay due to wave propagation in the B cell network. When drug treatments suppressed spontaneous activity in the B cell network, we activated B cells either by adding an NO donor (diethylamine/NO, DEA/NO) (Hrabie et al., 1993) to the bath or by treating the preparation with caged NO (nitrosylpentachlororuthenate, NPR) (Carter et al., 1993; Makings and Tsien, 1994) and applying uncaging flashes to the apical or basal region of the PC lobe by shutter-controlled localized epiillumination.

2.2. Model Description

The model consists of a spatially distributed network of bursting and nonbursting cells. Since the wave on the PC lobe appears to vary only along one spatial dimension, we have modeled the spatial distribution as a one-dimensional line of cells—21 cells of each type (see Fig. 1).

2.2.1. Bursting Cells. These are responsible for the local field potential and generate the oscillations. Since little is known of the currents responsible for the genesis of the spontaneous oscillations, we have made a fairly simple model with only three currents, a leak, a potassium current, and a T-type calcium current. Wang et al. (2001) have shown that calcium is the dominant inward current responsible for the activity of bursting neurons. There are two reasons we chose the T-type current instead of a simpler calcium current. First, the oscillations occur at very hyperpolarized potentials suggesting a low threshold calcium current. Secondly, the oscillation is very sensitive to NO. In a recent paper, Kawai and Miyachi (2001) showed that T-type calcium channels in olfactory receptor neurons are modulated by cGMP. NO is a powerful signalling molecule and has been shown to activate cGMP through several pathways (Ahern et al., 2002). Thus, we introduce a T-type calcium channel which is modulated by NO. The potassium current aids in the repolarization and keeps the magnitude of the bursts low. The leak plays an important role as follows. Watanabe et al. (2003) have recently shown that intracellular chloride is important in determining the direction of propagation of the waves. We

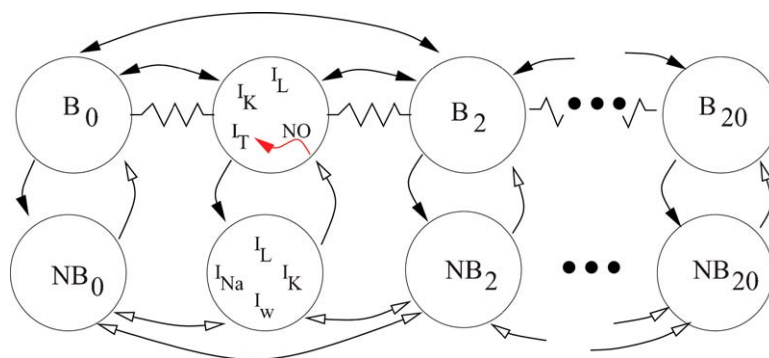


Figure 1. Schematic of the two-layer model. Bursting neurons, B_0, \dots, B_{20} are coupled with local electrical junctions and longer-range inhibitory coupling (black arrows). They have a T-type calcium current, potassium current, leak, and modulation through nitric oxide (NO) produced from the non-bursting cells (red arrow). Nonbursting neurons, NB_0, \dots, NB_{20} are coupled with excitatory chemical synapses (open arrows) and receive local inhibition from the bursting cells. They have fast sodium, potassium, leak, and a slower potassium current.

thus suppose that the leak consists of a chloride and a potassium leak. The gradient in intracellular chloride then acts to alter the reversal potential of the leak. At the apical end, the reversal potential is more depolarized than at the basal end. This results in an increase in the local frequency of the oscillation. The model equations for the voltage are:

$$C \frac{dV}{dt} = -g_L(V - E_L) - g_K n^4 (V - E_K) - g_{Ca} m^2 h V (V - E_{Ca}) - I_{couple}$$

where h , n are dynamical variables satisfying the usual gating equations, $\tau_x(V) dx/dt = x_\infty(V) - x$. The functions and parameters for these are given in the Appendix. The activation of the T-current satisfies:

$$m = 1 / (1 + \exp(-(V - V_{th})/6.2))$$

where $V_{th} = -58 - f[\text{NO}]$. $f = 2$ is a factor that converts concentration of nitric oxide [NO] into a millivolt shift. We do not include separate equations for the activation of cGMP through nitric oxide although such equations could easily be incorporated in the present formulation. Nitric oxide concentration obeys the following equations:

$$\frac{d[\text{NO}]}{dt} = ([\text{NO}]_{\text{back}} - [\text{NO}]) / \tau_{\text{NO}} + S$$

where we take $[\text{NO}]_{\text{back}} = 1 \mu\text{M}$ and $\tau_{\text{NO}} = 5000$ msec. The term S includes sources such as through the firing of the local NB cells. We have not included diffusion of [NO]; simulations (not shown) indicate that it makes little difference. Clearly, if $S = 0$ then diffusion will make no difference because of the uniform background concentration. We remark that a recent study by Jacklet and Tieman (2004) has shown that NO causes an increase in excitability of Aplysia neurons by suppressing a voltage-dependent potassium channel. This mechanism for action of NO on a model cell would result in similar behavior—by depolarizing the neuron, the frequency of oscillations would increase. For the network results that we present below, the details of how NO works are unimportant as long as it effects an increase in the burster frequency.

There are three terms in I_{couple} consisting of (i) nearest neighbor gap-junctional coupling; (ii) equal coupling through inhibition to the 5 neighbors on either side; and (iii) synaptic excitation from the local

nonbursting cell. Inhibitory synaptic currents have the form:

$$I_{\text{syn}} = g_{ii} s (V - E_i)$$

where

$$\frac{ds}{dt} = \alpha_i(V)(1 - s) - s/\tau_i.$$

Excitatory synapses have a similar form but with a different reversal potential and with the gate, s dependent on the local NB cell potential.

2.2.2. Non-Bursting Cells. Since these cells do not burst, only spiking currents were included:

$$C \frac{dV}{dt} = -g_L(V - E_L) - (g_K n^4 + g_W w)(V - E_K) - g_{Na} m^3 h (V - E_{Na}) - I_{\text{syn}} + I_{\text{stim}}.$$

We included a slow voltage-dependent potassium current, g_W for spike-frequency adaptation. The synaptic currents consisted of local inhibition from the bursting cell and recurrent excitatory connections from three neighbors on either side. Stimulation was meant to mimic the application of odorant, localized at discrete spatial points in the network and had the form:

$$I_{\text{stim}}(t) = -g_{\text{stim}} t e^{-t/40} (V - E_e)$$

where $E_e = 0$ is the reversal potential of the excitatory input stimulus.

2.2.3. Local Field Potential. “Local field potential” is obtained by adding the inhibitory synaptic currents of the 11 cells surrounding a given spatial location, and then passing through a low-pass filter with a time constant of 100 milliseconds.

3. Results

3.1. Distribution of Bursting Neurons

The distribution of bursting neurons within the PC lobe was determined by applying the activity-dependent vital dyes sulforhodamine 101 or Hoechst 33258 to the intact desheathed lobe and observing the pattern of stained neurons with TPSLM. Burster neurons have characteristic oval shaped somata and multiple processes projecting within the cell body layer (Fig. 2D),

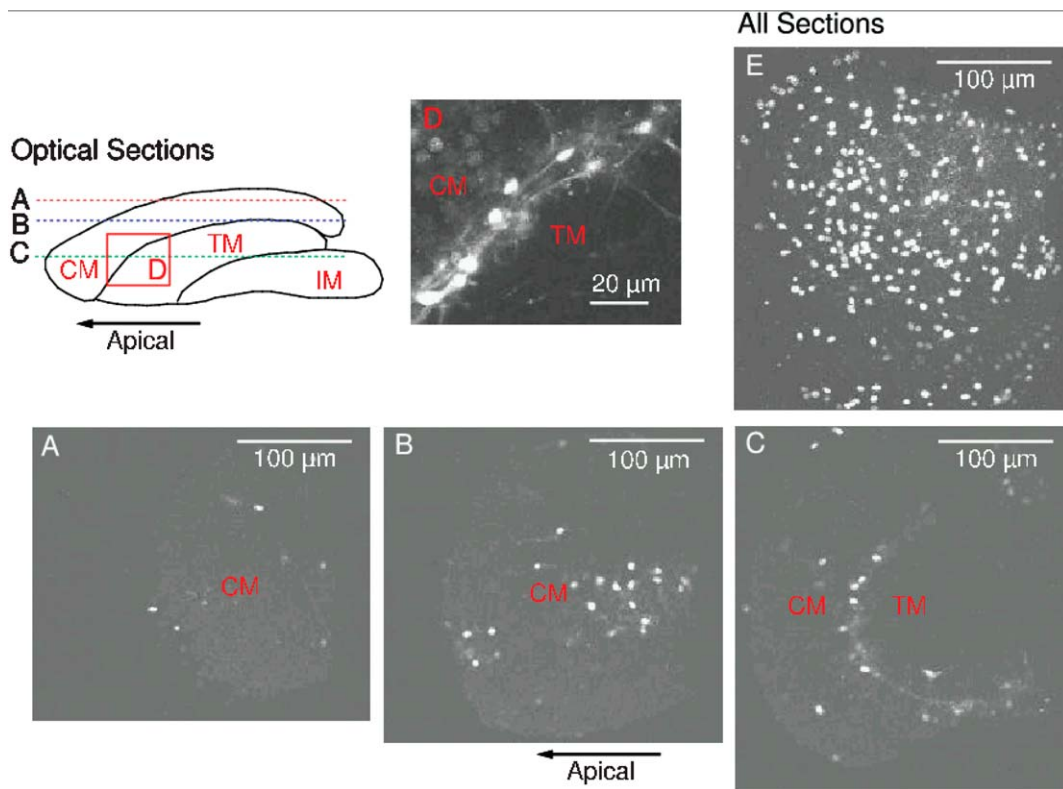


Figure 2. Distribution of burster neurons in the Limax procerebral lobe. Cells labeled by Hoechst 33258 are located in the cell body layer of the procerebral lobe immediately adjacent to the zone of termination of the olfactory afferent fibers. The PC lobe from a newly hatched slug was optically sectioned by two-photon laser scanning microscopy (Wang et al., 2001). Optical sections of the whole lobe with the cell layer facing the microscope objective are shown (A): for the surface layer, (B): 50 μm deep and (C): 100 μm deep. (D): A high resolution micrograph of labeled cells after sectioning the PC lobe at 150 μm thickness shows the oval nuclei and processes projecting within the cell layer, showing that the labeled cells are bursting neurons. (E): A projection of 150 optical sections at 1 μm intervals onto one image plane (NIH Image v.1.57) reveals all the labeled cells in this image volume, suggesting that there are about 300 bursting neurons in this PC lobe. CM cell mass, TM terminal mass, IM internal mass.

as determined by sharp electrode recording and intracellular dye injection (cf. Fig. 1 in Wang et al., 2001). Nonburster neurons have spherical somata and a single process projecting directly to the neuropil of the PC. Both sulforhodamine 101 and Hoechst 33258 stained burster neurons and revealed that the burster neuron somata are located in a 20 μm layer adjacent to the terminal neuropil (TM). Optical sections of the whole PC lobe with the cell layer facing the microscope objective also show that the bursting neurons are predominately located adjacent to the TM neuropil (Fig. 2A, B and C). A projection of 150 optical sections at 1 μm intervals onto one image plane reveals all the labeled B cells in the image volume (Fig. 2E). There are about 300 bursting neurons in this PC lobe from a newly hatched slug. The PC lobe is a site of active neurogenesis posthatching (Zakharov et al., 1998) so the adult PC lobe will

have a considerably larger population of B cells. Since we do not know the mechanism of selective Hoechst dye uptake into burster neurons and did not attempt an independent verification that all of the burster neurons were indeed stained, it is possible that the evidence of burster neuron density and distribution is an underestimate of the true density and distribution.

3.2. Response to ON Shock is Phase Dependent

The phase-dependence of responses of the B and NB cell networks in the Limax PC lobe is demonstrated most clearly by measuring responses to stimulation of the ON as a function of the phase of the spontaneous LFP oscillation at which the stimulus is given. Stimulation of the ON elicits a short-latency response

comprised of two components in the LFP record from the PC lobe cell body layer. The first peak in the LFP response to ON shock is due to currents set up by the volley of action potentials invading the PC lobe from the ON. This peak is not phase sensitive and is not sensitive to the calcium concentration in the bathing solution. The second peak in the LFP response to ON shock is phase sensitive and is reduced in low calcium saline (Gelperin and Tank, 1990). The size of the synaptic component of the LFP response to ON shock is minimal when the ON is shocked at a phase of 0.1 and increases linearly to an ON shock phase of 0.9 (cf. Fig. 3B in Gelperin and Tank, 1990). The input fibers from the ON synapse on NB cells (Inoue et al., 2000) so the synaptic component of the LFP response to ON shock arises from the summed EPSP in the population of NB cells contributing to the potential measured by the LFP electrode. Since the NB cell membrane potential is modulated by the 5–7 mV IPSP from the B cells with each cycle of the oscillation, the EPSP evoked in NB cells by the ON shock varies in amplitude during each cycle of the oscillation.

Single shocks of the ON also can elicit longer lasting changes in the frequency of the LFP oscillation, particularly at higher stimulus intensities (data not shown). As the ON shock is delivered at later and later phases of the ongoing LFP oscillation the NB cells are more and more likely to spike in response to the ON shock. NB spikes have two effects. They provide direct fast excitation of B cells and may trigger increased NO production by olfactory input fibers, which increases the burst rate of B cells. As shown in Fig. 2, the NO-sensitive B cell somata and processes are localized in the cell layer immediately adjacent to the neuropil where NO is likely to be released from input fiber neurites.

3.3. *Single Cell Behavior in Model*

A single B cell is capable of spontaneously oscillating. We have adjusted parameters so that the frequency varies from about 0.8 to 1.5 Hz. The frequency of oscillations depends on the two main parameters in the simulations: (i) the leak potential, E_L and (ii) the shift of the calcium current activation threshold, V_{th} . In Fig. 3A, we illustrate the potential of a single B cell for two values of the leak potential when $V_{th} = -60$ mV. We have included an inhibitory autapse since in the full spatial model, there is inhibition from neighboring neurons. For high and low values of the leak, there is a stable fixed point. Decreasing from a high leak potential, there

is a subcritical Hopf bifurcation (Fig. 3B) which turns around leading to a stable periodic orbit. Lower values of the leak restabilize the fixed point through another Hopf bifurcation. For $-83 < E_L < -80$, the fixed point is unstable and there is a stable periodic solution. The frequency of the limit cycles ranges from 1 to 1.5 Hz with a large linear region. Figures 3D and E show similar diagrams for variation of the calcium activation parameter, V_{th} with the leak fixed at -82 mV. As with the leak, there are two Hopf bifurcations. The frequency can range from less than 1 Hz up to 3 Hz. This range of frequencies matches the frequency range of the LFP oscillation measured in 150 μ m thick slices of the PC lobe cut along the apical-basal axis (cf. Fig. 4A in Ermentrout et al., 1998, and unpublished data). For values of leak below around -83 mV, the cells are too hyperpolarized for the voltage to cross the activation of the calcium current. On the other hand, when the leak potential is too positive, the cell is depolarized enough so that the T-current is inactivated.

Next, we consider a pair of cells, one a burster (B) and the second, a nonbursting (NB) cell. The B cell spontaneously oscillates and thus provides a phasic inhibition to the NB cell (Fig. 4). In our model, the inputs from the receptor neurons target the NB cells which dominate the lobe. As shown in Fig. 3B in Gelperin and Tank (1990), there is a consistent phase-dependence of the response of NB cells to inputs. This is shown for the model in Fig. 4. In Fig. 4A the input fails to make the NB cell spike and thus has no effect on the local B cell. The magnitude of the EPSPs evoked on the NB cell depend on the time of the input. Figure 4C shows the relative height of the EPSPs as a function of the time of the B-cell. Figure 4B shows that if the input comes late enough in the phase of the rhythm, then the NB cell can spike. This in turn increases the local B cell frequency, an effect which lasts for several cycles, as observed in experiments.

3.4. *Baseline Network*

Figure 5 shows a space-time picture of the potential of the B cells when there is a gradient in the leak ($E_L = -80$ mV at the apical end and -83 mV at the basal end) (cf. Fig. 3A). Nearest neighbor gap junctional coupling has strength 0.03 as does the inhibitory coupling. The network is active over about 60% of the cycle. Figure 5B shows the local field potential (LFP, see methods) at 3 sites (0 is most apical and 20 is most basal). We point out that in experiments, the apical LFP

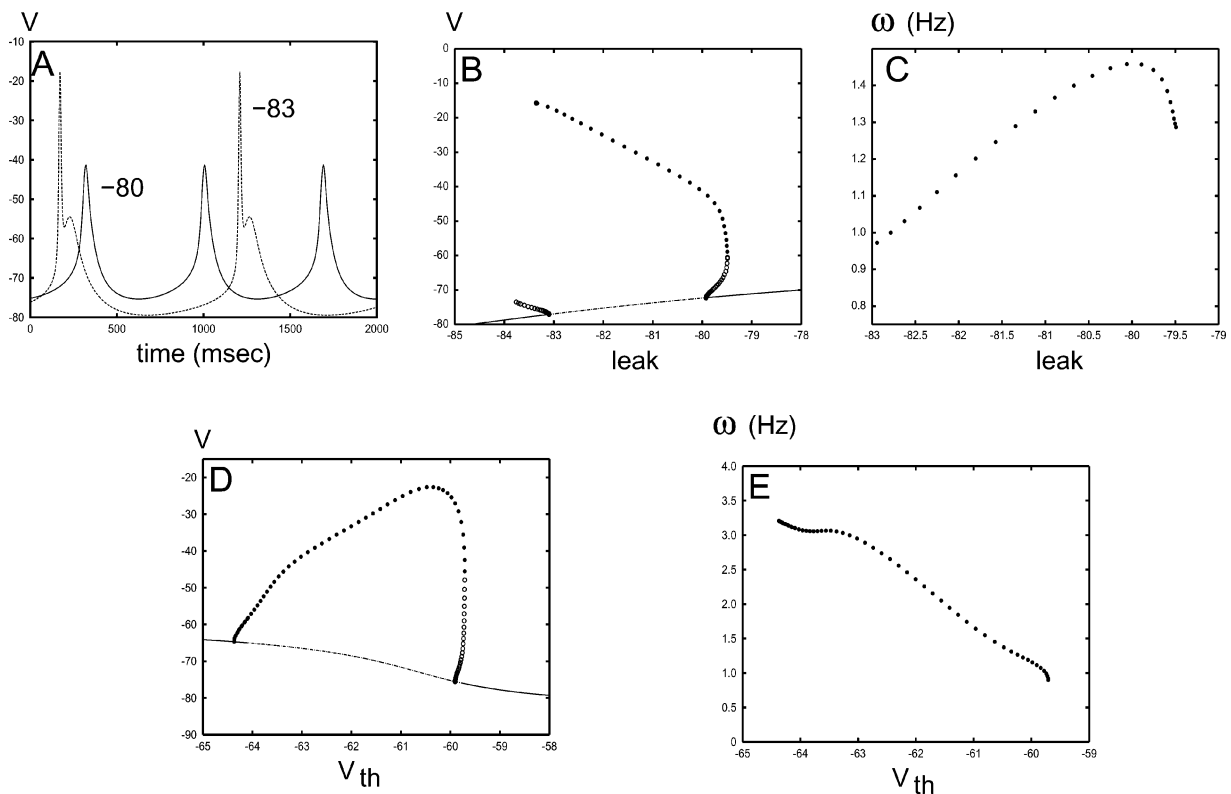


Figure 3. Properties of an individual B-cell. (A) Voltage of the B-cell for two different leaks $E_L = -83, -80$. The more depolarized leak has a higher frequency and a lower amplitude. (B) Bifurcation diagram showing the voltage as a function of the leak for $V_{th} = -60$ mV. (C) Frequency as a function of the leak. (D) Bifurcation diagram as a function of V_{th} , the activation threshold for the T-current for $E_L = -82$ mV. (E) Frequency as a function of the threshold.

has a larger magnitude than the basal end. This could be due to the fact that the cell layer is thicker at the apical end, so that the LFP may sum more currents. In our model, the faster cells have smaller amplitude action potentials.

3.5. Electrical and Chemical Coupling Among B Cells; Experiments

To guide further modeling, we explored the nature of neuronal coupling among B cells, both electrical and chemical. To characterize the effects of agents known to uncouple gap junctions, we used a Limax preparation that allowed direct assessment of gap junctional coupling between buccal neurons SB and B7 (Prior and Gelperin, 1977), as shown in Fig. 6. A single electrode voltage clamp maintains neuron SB at a constant membrane voltage while current pulses of varying amplitude are injected into neuron B7. The change in membrane

potential of neuron B7 was measured vs. the clamp current in neuron SB with and without 2 mM octanol or 100 μ M GA. Octanol reduced the conductance between buccal cells B7 and SB by 28%, while 100 μ M GA reduced B7-SB conductance by 17% (3 experiments, 2 preparations).

Having characterized the effects of GA and octanol on electrically coupled neurons in Limax, we then applied these gap junction blockers to the PC lobe and assessed their effects on both wave conduction and the local field potential in the B cell network. The preparation was bathed in 50 μ M NPR (caged NO donor) and uncaging flashes of 250 msec were applied to a 100 μ m diameter region either just apical to the apical LFP recording electrodes or just basal to the basal LFP recording electrode. Before the stimulus is given, the LFP is clearly visible in the PC lobe treated with saline but is completely absent in the GA-treated lobe. Thus, *gap junctions are required for the existence of a LFP*. The effects of the localized apical and basal NO

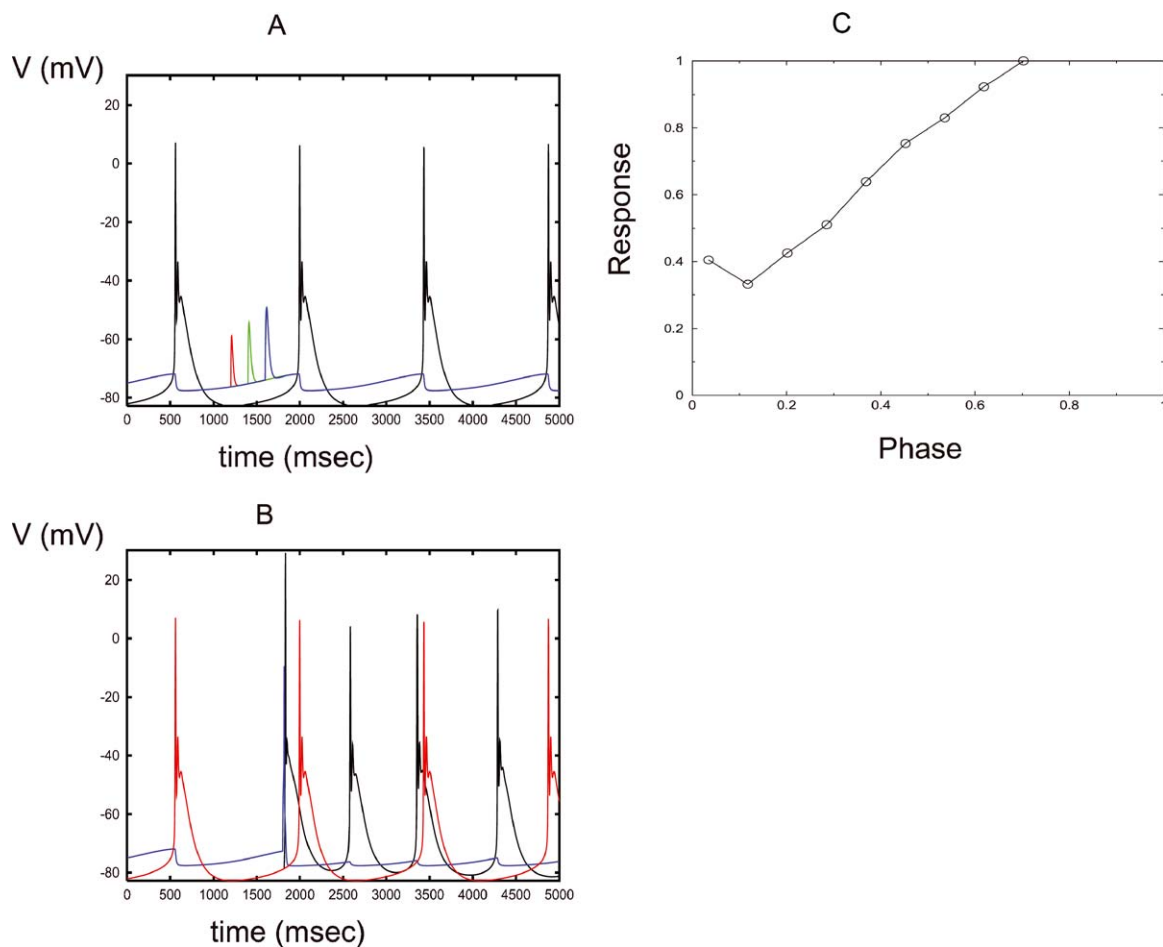


Figure 4. Phase dependence of the evoked EPSP onto NB cells. (A) Bursting cell (black) and nonbursting cell (colored) potentials for three different stimuli at $t = 1200, 1400, 1600$ milliseconds. (B) Stimulus at $t = 1800$ milliseconds is sufficient to cause firing of the NB cell (blue), and subsequent speeding up of the B cell rhythm (black) compared to the case of no stimulus (red). (C) Dependence of the relative EPSP size measured from base to peak (in Fig. A) as a function of the timing relative to the burst. For stimuli occurring later than about 70% of the cycle, the stimulus evokes a spike in the NB cell.

uncaging flashes when the lobe is in normal saline are shown in the upper part of Fig. 7. The apical flash increased activity at both apical and basal recording sites while the basal flash produced a strong effect at the basal site but a weaker effect at the apical site. Addition of $100 \mu\text{M}$ GA blocked the basal to apical propagation (except for a single peak occurring 2.3 seconds after the flash) but left intact the apical to basal propagation (Fig. 7, middle panels). This is in contrast to the control response to a basal flash recorded in normal saline, where small amplitude activity is evident in the apical record immediately after the basal flash and the first of two large amplitude apical events occurs with a latency of 0.5 sec after the flash. One possible ex-

planation for the reduced efficacy of GA in blocking apical-to-basal wave propagation versus the efficacy of GA in blocking basal-to-apical wave propagation seen in Fig. 7 is due to the asymmetry in the effectiveness of apical and basal uncaging flashes in normal saline. However, the simulations described below and illustrated in Fig. 8 have no such asymmetries and are explained below. Further addition of 5 mM PTX, which blocks glutamate-mediated chloride conductances in molluscs (Cleland, 1996), suppressed the remaining apical-to-basal propagating activity and rhythmic responding at the recording sites adjacent to the uncaging flash (Fig. 7, lower panels). Similar results were seen with 2 mM OCT. Both electrical and chemical synaptic

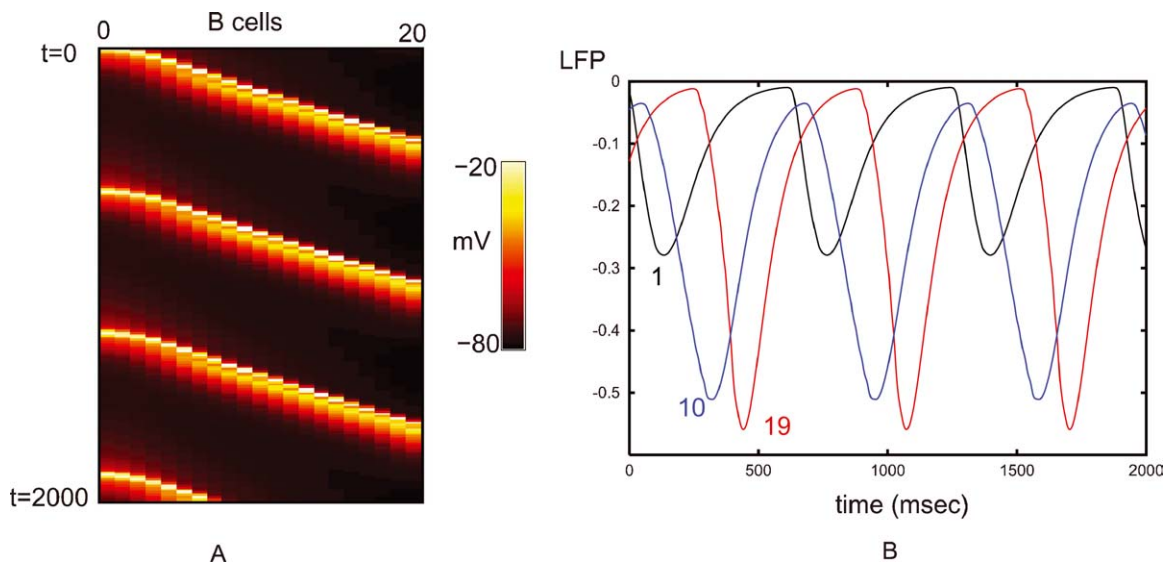


Figure 5. Normal wave behavior. (A) B-cell potentials in a space-time plot. Cell index (0–20) is horizontal and time runs downward. (B) Local field potentials of cells 1, 10, 19.

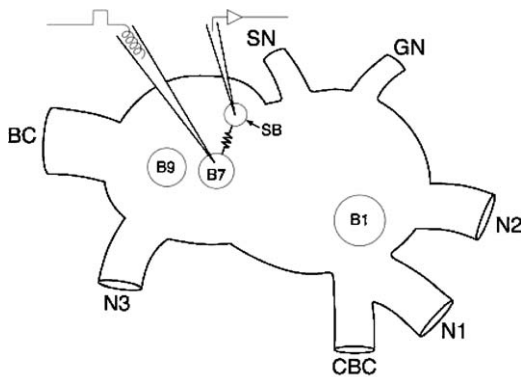


Figure 6. Buccal ganglion preparation used to measure the effects of gap junction uncoupling agents. B7, B9 = identified buccal motoneurons, SB = salivary burster neuron, B1 = identified buccal cell, BC = buccobuccal connective, CBC = cerebrobuccal connective, GN = gastric nerve, N1, N2, N3 = buccal nerve roots 1, 2, 3, SN = salivary nerve. Single electrode voltage clamp maintains SB at a constant V_m . Current pulses of varying amplitude are injected into B7. The change in V_m of neuron B7 is then plotted vs the clamp current flow in neuron SB.

transmission clearly play a role in propagation within the B cell network, which is also highly NO sensitive.

3.6. Effects of Local NO Depend on Location

Figure 8 illustrates a simulation in which the gap junctions are partially blocked and NO is incremented either

at the apical or the basal ends. At $t = 2000$, the NO concentration is raised from 1 to 2.5 at a single site to mimic the uncaging experiment. The LFP of sites 0 and 20 are shown before and after uncaging. The middle panel shows that apical uncaging has an effect which propagates to the basal end as in Fig. 7 in the middle panels. However Fig. 8 also shows that an increment in the basal NO, while transiently increasing the basal LFP, does not have any effect on the apical LFP. While apical application of NO has an effect on the basal LFP, there is no entrainment. That is, the apical and basal ends do not show transient phaselocking. (The gap junctions are not completely blocked so that the LFP remains in Figs. 8 and 9. Figure 11 shows complete blockage of the gap junctions.) This Fig. 8 also shows that NO has different effects on the amplitude of the LFP depending on whether it is applied basally or apically. This can be explained by looking at Fig. 3D which shows a nonmonotone dependence of the voltage amplitude on the T-current activation threshold. The value of V_{th} at which the amplitude peaks depends on the leak potential. For higher values of the leak potential this peak is shifted to the right. Cells at the apical end of the lobe are in the regime where decreasing V_{th} through application of NO decreases the amplitude while those at the basal end (more hyperpolarized) increase their amplitude when V_{th} is lowered. These differential effects also provide an explanation for the asymmetry in propagation with low gap junctions. NO speeds up

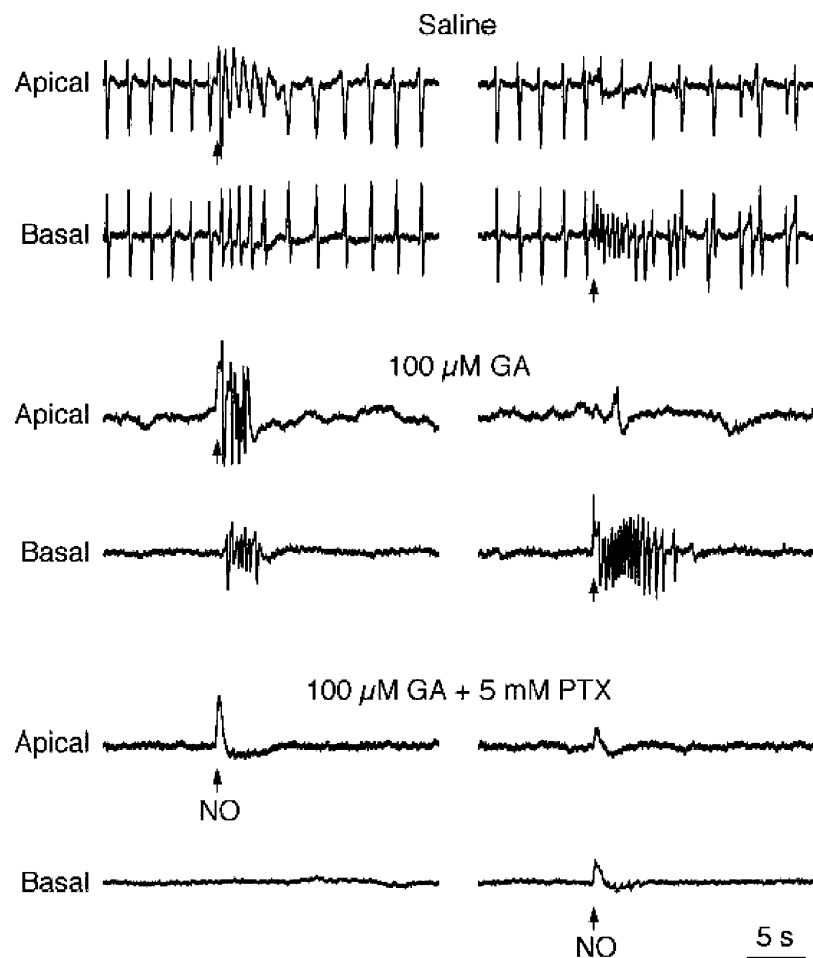


Figure 7. Effects of gap junctional blockers on wave propagation triggered by localized uncaging of nitric oxide at the apex (top trace in each pair of traces) or at the base (bottom trace of each pair of traces) of the PC lobe. $18\ \alpha$ glycyrrhetic acid (GA) blocks basal-apical wave propagation and picrotoxin (PTX) blocks local oscillation to a localized nitric oxide (NO) stimulation. GA blocks basal-apical waves but not apical-basal waves. NO uncaging flashes were delivered with the preparation in saline, $100\ \mu\text{M}$ $18\ \alpha$ glycyrrhetic acid (GA), and $100\ \mu\text{M}$ GA + $5\ \text{mM}$ picrotoxin (PTX).

the oscillation. The apical end is already faster than the basal end so that the increase in frequency at the apical end enhances this difference and is propagated. However, speeding up the basal end (via application of NO at the basal end) must result in a wave that propagates in the opposite direction from the control case. The increase in basal frequency is transient and so does not last long enough to propagate down the entire lobe.

The location dependence is somewhat different when the gap junctions are not blocked. Figure 9 shows the same experiments with no blocking of the gap junctions and shows the potentials of all the B cells. For

stimuli at the apical end, an already faster apical cell speeds up even more and only partial entrainment is possible. For stimuli at the basal end, there is a speed up in the local oscillation. But this phase wave is unable to propagate across the lobe in time to entrain the apex before the basal B cells return to their slow frequency. We predict that a sustained NO increase at the basal end should eventually entrain the whole lobe. In contrast, full entrainment through the apical end seems difficult. Stimulating the middle of the lobe speeds it up and the resulting phase wave is able to propagate to both ends of the lobe resulting in transient phaselocking across the whole lobe.

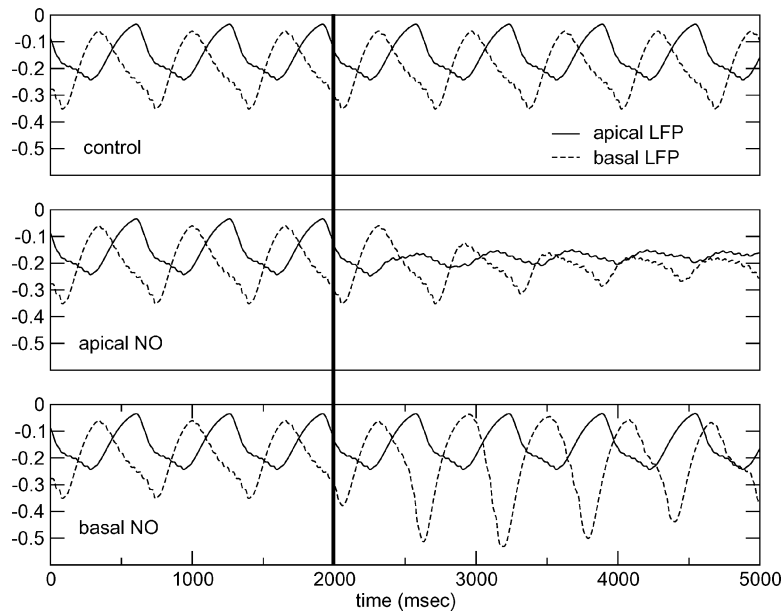


Figure 8. The effects of a local increase in NO depend on location in reduced gap junction models. Control shows LFP at sites 4 and 16 corresponding to apical and basal respectively with gap junctions partially blocked. At $t = 2000$ (dark line), NO is increased at site 0 (apical NO) or at site 20 (basal NO). Apical increases have an effect on the basal LFP, but not vice versa.

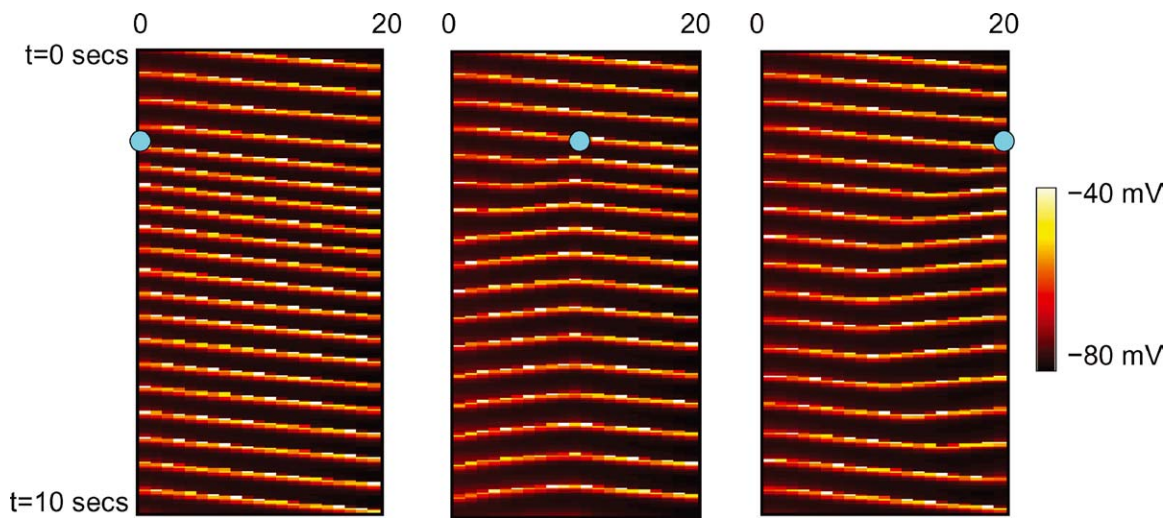


Figure 9. Space-time plots of the effect of local NO application with gap junctions intact. Plots show the potential of the B cells. Blue circle shows application of increased NO on each plot at $t = 2$ seconds.

3.7. Transient Synchrony

As we saw in Fig. 4, the response of an NB cell depends on the timing of the inputs with respect to the phase of the B cell oscillation. In our model of the NB cell layer, there are fast excitatory connections between NB cells and local recurrent connections with the spatially cor-

responding B cells. If a stimulus is timed correctly and at the correct location, it can lead to transient synchronization of the B cells as observed in local field potentials shown in Ermentrout et al. (1998). Figure 10A shows such a correctly timed stimulus. At the point of the arrow, site 10 is stimulated with a brief excitatory current. This is timed so that the cell fires and this in

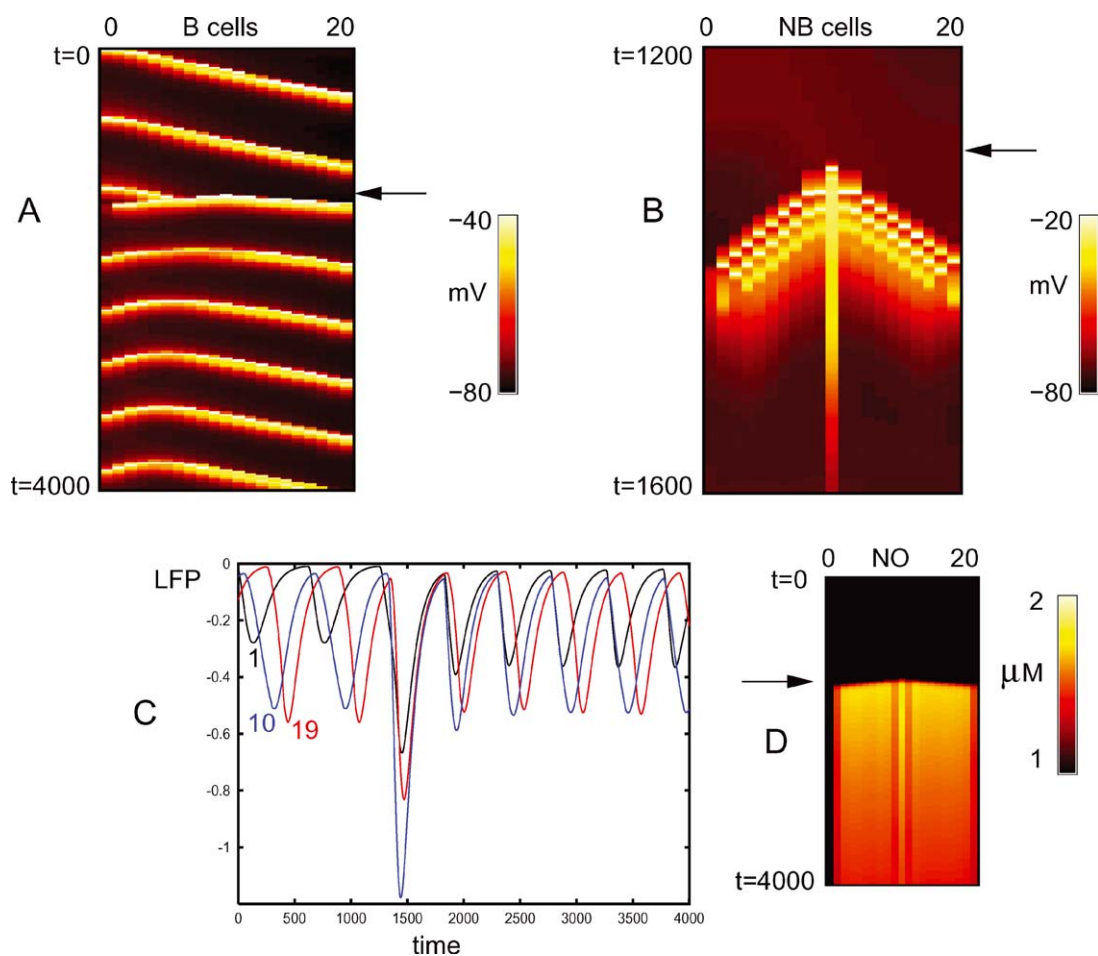


Figure 10. Transient synchrony due to excitation of an NB cell. (A) shows the space-time plot of the B cells. (B) shows an expanded view of the behavior of the NB cells. They generate a very fast wave of excitation which synchronizes the B cells. (C) Local field potential taken at sites 1, 10, and 19. Note transient synchrony and speed up of the oscillation. The latter is due to the production of NO associated with the firing of the NB cells. (D) NO wave is responsible for the increase in LFP frequency.

turn must excite the neighboring NB cells. If this fast wave of excitation can advance through the NB cells, it can excite the B cells causing an almost synchronous firing. However, even if the excited NB cell fires, depending on the state of the wave of inhibition, the NB wave can fail to propagate in one direction or another due to the timing of the inhibition. Figure 10C shows the LFP at three sites before and after the excitation. Note that it takes several cycles of the B cell oscillation before the LFP returns to the prestimulus phase lags. This can also be seen in Fig. 10A through the B cell potentials. Figure 10B shows an expanded view of the potentials of the NB cells during the wave. Note that the wave of excitation is very fast and takes only about 100 msec to reach the boundaries from the edges. (A

way to think of what this means in terms of the velocity is that each NB cell communicates to 2 neighbors on either side, so that from the middle to the end is 5 synaptic footprints—the velocity is thus 100 footprints per second. Relative to the phase wave at resting conditions, the NB excitation velocity is 5–6 times faster than the oscillating wave.) When NB cells fire, they release NO which accounts for the transient increase in frequency after excitation. Figure 10D shows the concentration of NO in space and time after the excitation.

3.8. Blocking gap Junctions Disrupts the Rhythm

Experimental results in Fig. 7 show that the LFP is dramatically reduced when gap junctions are blocked.

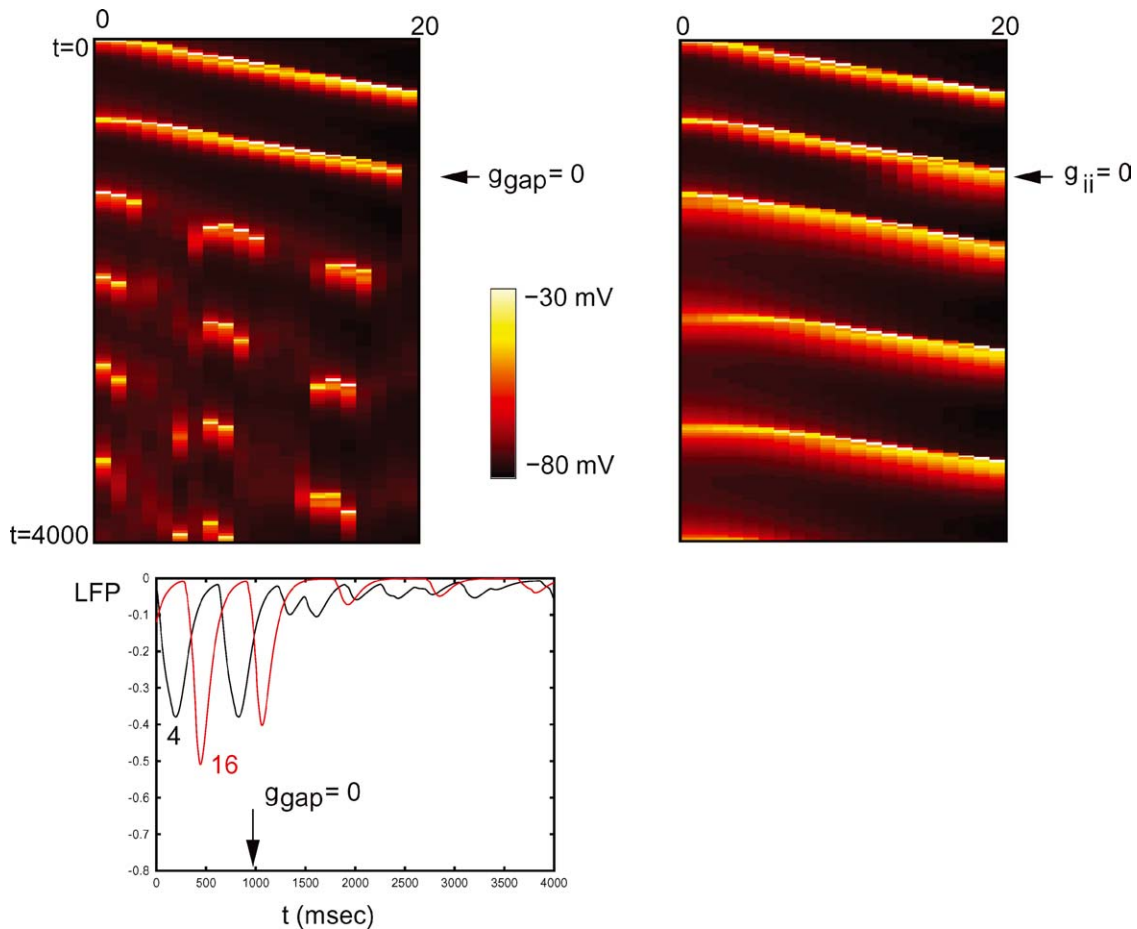


Figure 11. Role of coupling on the wave. At $t = 1000$, the coupling is disrupted. When gap junctions are blocked ($g_{\text{gap}} = 0$; left panel) the wave is disrupted and the local field potential is greatly diminished (lower left; $j = 4$ denoted in black and $j = 16$ denoted in red). Blocking the inhibition ($g_{ii} = 0$; right panel), slows the wave down but has little effect on its structure. (LFP is zero since it is determined from the inhibitory synaptic potentials.)

Figure 11 shows what happens to the wave if the gap junctions are completely blocked. The LFP shows a 10-fold decrease in magnitude. This is due to the sparsity of firing of the B cells which is shown in the space-time plot. Many of the cells are silent. We suggest that this silence is due to the inhibition from other B cells and that if this is blocked, more B cells will fire. However, the firing will be irregular and uncoupled from other B cells, so that the LFP should remain small. Blocking the inhibition slows the rhythm down but the waves persist. The slowing down is a consequence of the fact that the inhibition allows the inactivation gate of the calcium T-current to recover more quickly.

Curiously, the wave remains if we remove the gradient in the leak potential and simultaneously lower the

strength of the gap junctions. This is shown in Fig. 12. Note that the phase gradient is not as steep as in the normal wave. It can be steepened by lowering the gap junction strength. But this cannot be lowered too much or the wave will break up. The mechanism for the appearance of the wave in absence of the gradient will be the subject of a more detailed analysis in a later paper. Briefly, for this particular neural oscillator, the inhibitory synaptic coupling tends to destabilize the synchronous state while the gap junctions stabilize it. Since the synaptic coupling extends beyond the local gap junctional coupling, the most stable phase pattern is a traveling wave. Of course, if the gap junction strength is too strong, then the network synchronizes and if it is too weak, there is a break-up of the network into either a

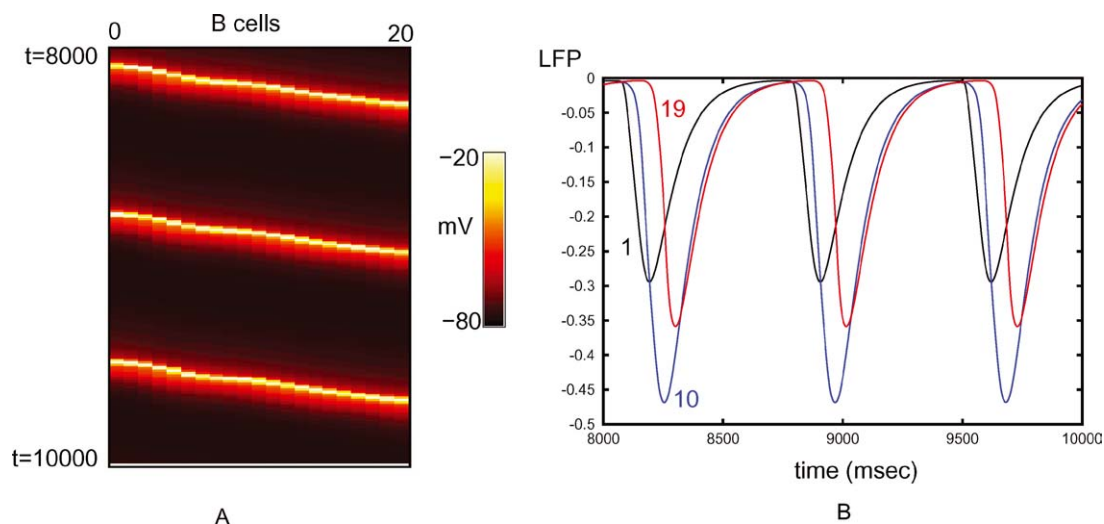


Figure 12. The chloride gradient is not necessary for wave formation. $E_L = -81.5$ mV uniformly across the network and the gap junctions are reduced from 0.03 to 0.015 in strength. (A) Potential of the B cells and (B) local field potentials at 3 sites in the network.

clustered or asynchronous state. The gradient enhances the wave-like behavior and can produce a wave even if the inhibition is blocked. Without the gradient, the wave can also propagate in the opposite direction, depending on initial conditions, thus, the gradient also fixes the direction of the wave.

4. Discussion

Our biophysical models of B and NB cell arrays are able to reproduce several of the measured properties of the PC lobe, both its intrinsic dynamics and responses to input from the olfactory nerve. Odor inputs can produce synchrony if they occur at a certain phase of the oscillation, are sufficiently long in duration, have a broad spatial distribution of activation within the PC lobe or if there is sufficiently strong excitatory coupling between NB cells. Normal odor packets resulting from turbulent flow downwind of a point source of odor are typically several seconds in duration (Murlis et al., 1990, 1992). The distribution of activation within the PC lobe due to odor stimulation is unknown in detail but may be restricted to band-like regions based on odor learning-dependent Lucifer yellow band formation in the PC lobe of *Limax* (Ermentrout et al., 2001; Gelperin, 1999; Kimura et al., 1998a). The strength of NB-NB neuron coupling could be modulated by one or more of the 21 neurotransmitters present in the PC lobe (Gelperin, 1999) to enhance the effectiveness of

brief local inputs in producing synchrony in the B cell network.

Treating the B cell network as comprised of morphologically and biophysically homogeneous neurons is an oversimplification. Recent two-photon imaging experiments revealed two morphological classes of B neurons and two distinct axonal propagation speeds along B cell neurites (Wang et al., 2001). Varicose and smooth B cell neurites were found after loading B neurons with calcium green dextran. Also, varicose B neurons with neurites propagating activity transversely across the PC lobe had a propagation speed of $4.3 \mu\text{m}/\text{ms}$ while smooth B cell neurites arrayed along the apical-basal axis had a propagation speed of $1.3 \mu\text{m}/\text{ms}$. The propagation speed of action potentials in smooth B cell neurites, which does not include synaptic delays, is close to the measured speed of propagation of the apical-basal activity wave ($1.1 \mu\text{m}/\text{ms}$) (Kleinfeld et al., 1994).

The PC lobe contains both NO synthesizing and carbon monoxide (CO) synthesizing neurons (Gelperin et al., 2000, 2001). Since calcium and calmodulin are essential for activity of the constitutive cytosolic NO synthase found in neurons (Bredt and Snyder, 1990; Huang et al., 1997; Korneev et al., 1998), the increased intracellular calcium due to spiking in NB cells may increase NO production and thereby excite neighboring B cells. It is also possible that neurites of olfactory receptor neurons projecting to the neuropil region immediately adjacent to the cell body layer contain nitric oxide synthase (NOS) (Cooke et al.,

1994; Sanchez-Alvarez et al., 1994) that is activated by spike activity in olfactory afferents. A role for NO in chemosensory activation of feeding in molluscs has been demonstrated (Elphick et al., 1995). The role of NO generation in olfactory function can be studied using suppression of the neuronal NO synthase gene with double-stranded RNA, as recently demonstrated for NO-dependent feeding behavior in the snail *Lymnaea stagnalis* (Korneev et al., 2002). The CO containing neurites in the PC lobe are located in the most basal region of the neuropil making it less likely that activity-dependent CO generation amplifies NB cell activation of B cells.

The B cells in our model have a T-type calcium conductance whose activation curve is shifted by NO. Both B (Wang et al., 2001) and NB (Gelperin and Flores, unpublished) cells have calcium action potentials and both B (Fujie et al., 2002) and NB (Gelperin, 1994) cells contain NOS likely to be activated by calmodulin after spike mediated calcium entry. The close proximity of B and NB somata in the cell layer of the PC lobe insures that B cell conductances will be affected by NO production originating in both B and NB cells.

Networks of bursting inhibitory interneurons play a critical role in shaping the periodicity of principle cell responses in cortex (Buzsaki and Chrobak, 1995; Freund and Buzsaki, 1996; Zhang et al., 1998). Electrical coupling mediated by gap junctions (Bennett, 1997) is an essential component of the coupling of these cortical inhibitory interneurons (Beierlein et al., 2000; Skinner et al., 1999). The B cells in the Limax PC lobe are coupled by both chemical and electrical synapses, a design feature they share with cortical inhibitory networks (Gelperin, 1999). However, as shown recently by Bem and Rinzel (2004), mutual inhibition between bursting cells can lead to anti-phase behavior; that is, a pair of mutually coupled bursters fires out of phase. As with their model, gap junctions resynchronize a pair of identical cells coupled with reciprocal inhibition in our model. Thus, the interplay between gap junctions, inhibition, and a frequency gradient in the present model is quite different from the roles played by gap junctions and inhibition in other models. Here, there is a "competition" between the desynchronizing effects of inhibition and the synchronizing effects of gap junctions. The result of this interaction is a phase-gradient. The frequency gradient both enhances this and provides a bias in the apical to basal direction. This bias can be over-ridden (see, e.g., Fig. 9 right panel) with sufficient transient input at the basal end.

The compounds OCT and GA have been used in a variety of studies of gap junctional coupling among vertebrate neurons (Bennett, 1997; Largo et al., 1997; Ozog et al., 2002). Molluscan gap junctions are demonstrably different than vertebrate gap junctions in their sensitivities to blockers (Bodmer et al., 1988). Identification of the connexin (Evans and Martin, 2002) or innexin (Phelan and Starich, 2001; Panchin et al., 2000) subunits expressed in neurons of the Limax PC lobe would allow identification of a more selective blocker of Limax gap junctional communication. Simoes-de-Souza and Roque (2004) have recently suggested a role for gap junctions in the olfactory epithelium of vertebrates. By using a computational model, they show that electrical coupling between receptor neurons can be tuned so that odor stimulation propagates as a wave of excitation across the epithelium producing a sustained response to the inputs.

Bazhenov et al. (2001) have recently proposed a model for synchronous oscillations observed in the locust antennal lobe. Like our model, theirs comprises excitatory cells that have fast spiking currents and inhibitory cells that have only a T-type calcium channel for depolarization. In the absence of odorant stimuli, their model is quiescent; in particular, the inhibitory neurons (analogs of our B-cells) do not fire unless they are depolarized. Thus odorants produce oscillations by exciting the PN (excitatory) cells that turn on the LN (inhibitory cells) and produce an oscillation. Synchrony is a consequence of the excitatory-excitatory interactions, the mechanism of which is similar to other cortical models (Traub and Miles, 1991). Oscillations are intrinsic in our model and synchronization comes from the fast interactions between excited NB cells.

The activity wave which travels from apex to base in the PC lobe is used to separate the odor memory representations set up by associative conditioning experiments in which odors are used as the conditioned stimulus (Ermentrout et al., 2001; Kimura et al., 1998a). Activity waves are also found in central olfactory structures in vertebrates (Freeman, 1978; Lam et al., 2000) and in visual cortex of turtle (Prechtl et al., 1997, 2000). Computational studies on networks of coupled neuronal oscillators show that traveling waves are an emergent property of systems with spatially restricted (nearest neighbor) connectivity (Kopell and Ermentrout, 1986). Ermentrout and Kleinfeld (2001) have recently suggested that the continuum of phase shifts during epochs with traveling waves provides a means to scan the incoming sensory stream for novel

features. The rhythmic inhibition of principle cells in cortex or NB cells in the PC lobe enhances the temporal correlations among the subset of neurons responding to a sensory input, which may contribute an essential temporal response synchrony needed to identify the stimulus (Teyke and Gelperin, 1999; Wehr and Laurent, 1996).

Inhibitory responses of NB neurons in the Limax PC lobe to 4 natural complex odorants have been described based on intracellular recordings from NB cells in an in vitro nose-brain preparation (Murakami et al., 2004). A similar in vitro preparation can be assessed for inhibitory responses to aversive odor stimuli using contraction of the mantle muscle (Inoue et al., 2004). If innately attractive odors that become aversive due to odor conditioning also lead to contraction of the mantle muscle, the role of the PC lobe in such learned alterations of odor meaning can be directly assessed.

The model makes several specific predictions about biophysical mechanisms underlying the generation of rhythmic wave propagation in the PC lobe. The presence and density of T-type calcium channels can be tested by use of recently developed selective blockers (Huang et al., 2004), in addition to voltage clamp studies aimed at isolating the low-voltage-activated T-type calcium channel (Yunker, 2003). The presence of localized nitric oxide production during each cycle of wave propagation can be tested using miniaturized NO-sensitive electrodes with time constants of NO response fast enough to reveal 1 Hz variations (Buerk et al., 2003).

Appendix: Model Parameters

Each B cell has the form:

$$C \frac{dV}{dt} = -g_L(V - E_L) - g_K n^4(V - E_K) - g_{Ca} m^2 h(V - E_{Ca}) + I_{gap} + I_{syn}$$

n , h obey equations of the form:

$$\begin{aligned} \frac{dn}{dt} &= .075[a_n(V)(1 - n) - b_n(V)n] \\ \frac{dh}{dt} &= 1.125(h_\infty(V) - h)/\tau_h(V) \end{aligned}$$

with

$$\begin{aligned} a_n(V) &= .032(-48 - V)/(\exp(-(48 + V)/5) - 1) \\ b_n(V) &= .5 \exp(-(43 + v)/40) \end{aligned}$$

$$h_\infty(V) = 1/(1 + \exp((v + 86)/4))$$

$$\begin{aligned} \tau_h(V) &= \text{if } (V < (-80)) \\ &\quad \text{then } (\exp((V + 470)/66.6)) \\ &\quad \text{else } (28 + \exp((V + 25)/ - 10.5)) \end{aligned}$$

The activation gate for the T-type calcium current has the form:

$$m(V) = 1/(1 + \exp(-(V + 58 + 2[\text{NO}])))$$

where $[\text{NO}]$ is the local concentration of nitric oxide. $[\text{NO}]$ satisfies

$$\frac{d[\text{NO}]}{dt} = (1 - [\text{NO}] + 75s_{NB})/5000$$

where s_{NB} is the synaptic gate of the local NB cell (see below). The standard parameters are $C = 3$, $g_K = 5$, $g_L = .025$, $g_{Ca} = 2$, $E_K = -90$, $E_{Ca} = 140$ and E_L is a linear gradient starting at -80 at the apical end and ending at -83 at the basal end. All conductances are in mS/cm^2 , potentials in millivolts, capacitance in $\mu\text{F}/\text{cm}^2$ and times in millisecond. Gap junction coupling was to nearest neighbors, $I_{gap} = g_{gap}(V_{j+1} - 2V_j + V_{j-1})$ where typically, $g_{gap} = .03$. Synaptic inhibition between B cells was distributed equally over the cell itself and its 5 neighbors on either side; while synaptic excitation from the NB cells was only local.

$$I_{syn} = -\frac{g_{ii}}{11} \sum_{k=-5}^5 s_{B,j+k}(V_j + 78) - g_{ei} s_{NB,j} V_j.$$

We chose $g_{ei} = .05$ and $g_{ii} = .03$. The synaptic gates satisfy

$$\begin{aligned} \frac{ds_B}{dt} &= 0.1/(1 + \exp(-(V + 45)/5)) - s_B/100 \\ \frac{ds_{NB}}{dt} &= (1 - s_{NB})/(1 + \exp(-(V_{NB} + 20)/2)) \\ &\quad - s_{NB}/25 \end{aligned}$$

where V is the local B cell potential and V_{NB} the local NB cell potential. The NB cells satisfy:

$$\begin{aligned} C \frac{dV_{NB}}{dt} &= -g_L(V_{NB} - E_L) - (g_K n^4 + g_w w)(V_{NB} - E_K) \\ &\quad - g_{Na} m^3 h(V_{NB} - E_{Na}) + I_{syn} + I_{stim} \end{aligned}$$

where $g_L = .04$, $g_{Na} = 12$, $g_K = 5$, $g_w = .25$, $E_K = -90$, $E_{Na} = 55$, $E_L = -65$. n , m , h gates

satisfy $dx/dt = a(1 - x) - bx$ and w satisfies $\tau dw/dt = w_\infty - w$ where

$$\begin{aligned} a_m(V_{NB}) &= 0.091(V_{NB} + 38)/ \\ &\quad (1 - \exp(-(V_{NB} + 38)/5)) \\ b_m(V_{NB}) &= -0.062(V_{NB} + 38)/ \\ &\quad (1 - \exp((V_{NB} + 38)/5)) \\ a_h(V_{NB}) &= 0.016 \exp((-55 - V_{NB})/15) \\ b_h(V_{NB}) &= 2.07/(1 + \exp((17 - V_{NB})/21)) \\ a_n(V_{NB}) &= 0.01(-45 - V_{NB})/ \\ &\quad (\exp((-45 - V_{NB})/5) - 1) \\ b_n(V_{NB}) &= 0.17 \exp((-50 - V_{NB})/40) \\ w_\infty(V_{NB}) &= 1/(1 + \exp(-(V_{NB} + 35)/10)) \\ \tau_w(V_{NB}) &= 1000/(3.3(\exp((V_{NB} + 35)/20) \\ &\quad + \exp(-(V_{NB} + 35)/20))) \end{aligned}$$

Each NB cell receives synaptic inhibition from a local B cell, synaptic excitation from itself and 2 neighbors on each side and external stimuli:

$$\begin{aligned} I_{syn} &= -g_{ie} s_B (V_{NB} + 78) \\ &\quad - g_{ee} \sum_{k=-2}^2 s_{NB,j+k} V_{NB} \\ I_{stim} &= -A_j (t - t_{on}) \exp(-(t - t_{on})/40) V_{NB} \end{aligned}$$

where t_{on} is the onset time of the stimulus and A_j is 0.1 mS if the j th NB cell is stimulated.

Complete equations and parameter files are available from GBE.

Acknowledgments

Alan Gelperin was supported by NIH MH56090 and GBE was supported by NSF DMS 0209942.

References

- Ahern GP, Klyachko VA, Jackson MB (2002) cGMP and S-nitrosylation: Two routes for modulation of neuronal excitability by NO. *Trends Neurosci.* 25: 510–517.
- Bazhenov M, Stopfer M, Rabinovich M, Abarbanel HD, Sejnowski TJ, Laurent G (2001) Model of cellular and network mechanisms for odor-evoked temporal patterning in the locust antennal lobe. *Neuron* 30: 569–581.
- Beierlein M, Gibson JR, Connors BW (2000) A network of electrically coupled interneurons drives synchronized inhibition in neocortex. *Nature Neurosci.* 3: 904–910.
- Bem T, Rinzel J (2004) Short duty cycle destabilizes a half-center oscillator, but gap junctions can restabilize the anti-phase pattern. *J. Neurophysiol.* 91: 693–703.
- Bennett MV (1997) Gap junctions as electrical synapses. *J. Neurocytol.* 26: 349–366.
- Bodmer R, Verselis V, Levitan IB, Spray DC (1988) Electronic synapses between *Aplysia* neurons in situ and in culture: Aspects of regulation and measurements of permeability. *J. Neurosci.* 8: 1656–1670.
- Bou-Flores C, Berger AJ (2001) Gap junctions and inhibitory synapses modulate inspiratory motoneuron synchronization. *J. Neurophysiol.* 85: 1543–1551.
- Bredt DS, Snyder SH (1990) Isolation of nitric oxide synthase, a calmodulin requiring enzyme. *Proc. Natl. Acad. Sci. USA* 87: 682–685.
- Buerk D, Ances B, Greenberg J, Detre J (2003) Temporal dynamics of brain tissue nitric oxide during functional forepaw stimulation in rats. *Neuroimage.* 18: 1–9.
- Buzsaki G, Chrobak JJ (1995) Temporal structure in spatially organized neuronal ensembles: A role for interneuronal networks. *Curr. Opin. Neurobiol.* 5: 504–510.
- Carter TD, Bettache N, Ogden D, Trentham DR (1993) Photochemical release of nitric oxide from ruthenium nitrosyl trichloride: Relaxation of rabbit isolated aortic rings mediated by photo-release of nitric oxide. *J. Physiol.* 467: 165P.
- Cleland TA (1996) Inhibitory glutamate receptor channels. *Mol. Neurobiol.* 13: 97–136.
- Cooke IRC, Edwards SL, Anderson CR (1994) The distribution of NADPH-diaphorase activity and immunoreactivity to nitric oxide synthase in the nervous system of the pulmonate mollusc *Helix aspersa*. *Cell Tissue Research* 277: 565–572.
- Copeland J, Gelperin A (1983) Feeding and a serotonergic interneuron activate an identified autoactive salivary neuron in *Limax maximus*. *Comp. Biochem. Physiol.* 76A: 21–30.
- Davidson JS, Baumgarten IM (1988) Glycyrhethinic acid derivatives: A novel class of inhibitors of gap-junctional intercellular communication. Structure-activity relationships. *J. Pharmacol. Exp. Ther.* 246: 1104–1107.
- Delaney KR, Gelperin A, Fee MS, Flores JA, Gervais R, Tank DW, Kleinfeld D (1994) Waves and stimulus-modulated dynamics in an oscillating olfactory network. *Proc. Natl. Acad. Sci. USA* 91: 669–673.
- Denk W, Svoboda K (1997) Photon upmanship: Why multiphoton imaging is more than a gimmick. *Neuron* 18: 351–357.
- Dorries KM, Kauer JS (2000) Relationship between odor-elicited oscillations in the salamander olfactory epithelium and olfactory bulb. *J. Neurophysiol.* 83: 754–765.
- Elphick MR, Kemenes G, Staras K, O'Shea M (1995) Behavioral role for nitric oxide in chemosensory activation of feeding in a mollusc. *J. Neurosci.* 15: 7653–7664.
- Ermentrout B (2002) *Simulating, Analyzing, Animating Dynamical Systems: A Guide to XPPAUT for Researchers and Students*, SIAM, Philadelphia, PA.
- Ermentrout B, Flores J, Gelperin A (1998) Minimal model of oscillations and waves in the *Limax* olfactory lobe with tests of the model's predictive power. *J. Neurophysiol.* 79: 2677–2689.
- Ermentrout B, Wang JW, Flores J, Gelperin A (2001) Model for olfactory discrimination and learning in *Limax* procererebrum incorporating oscillatory dynamics and wave propagation. *J. Neurophysiol.* 85: 1444–1452.

- Ermentrout GB, Kleinfeld D (2001) Traveling electrical waves in cortex: Insights from phase dynamics and speculation on a computational role. *Neuron* 29: 33–44.
- Evans WH, Martin PEM (2002) Gap junctions: Structure and function. *Mol. Membrane Biol.* 19: 121–136.
- Freeman WJ (1978) Spatial properties of an EEG event in the olfactory bulb and cortex. *Electroenceph. Clin. Neurophysiol.* 44: 586–605.
- Freund TF, Buzsáki G (1996) Interneurons of the hippocampus. *Hippocampus.* 6: 347–470.
- Fujie S, Aonuma H, Ito I, Gelperin A, Ito E (2002) The nitric oxide/cyclic GMP pathway in the olfactory processing system of the terrestrial slug *Limax maximus*. *Zoolog. Sci.* 19:15–26.
- Gelperin A, Tank DW (1990) Odor-modulated collective network oscillations of olfactory interneurons in a terrestrial mollusc. *Nature* 345: 437–440.
- Gelperin A (1994) Nitric oxide mediates network oscillations of olfactory interneurons in a terrestrial mollusc. *Nature* 369: 61–63.
- Gelperin A (1999) Oscillatory dynamics and information processing in olfactory systems. *J. Exp. Biol.* 202: 1855–1864.
- Gelperin A, Flores J, Raccuia-Behling F, Cooke IRC (2000) Nitric oxide and carbon monoxide modulate oscillations of olfactory interneurons in a terrestrial mollusc. *J. Neurophysiol.* 83: 116–127.
- Gelperin A, Kao JPY, Cooke IRC (2001) Gaseous oxides and olfactory computation. *Amer. Zool.* 41: 332–345.
- Gervais R, Kleinfeld D, Delaney KR, Gelperin A (1996) Central and reflex neuronal responses elicited by odor in a terrestrial mollusc. *J. Neurophysiol.* 76: 1327–1339.
- Hrabie JA, Klose JR, Wink DA, Keefer LK (1993) New nitric oxide-releasing zwitterions derived from polyamines. *J. Org. Chem.* 58: 1472–1476.
- Huang S, Kerschbaum HH, Engel E, Hermann A (1997) Biochemical characterization and histochemical localization of nitric oxide synthase in the nervous system of the snail, *Helix pomatia*. *J. Neurochem* 69: 2516–2528.
- Huang L, Keyser B, Tagmose T, Hansen J, Taylor J, Zhuang H, Zhang M, Ragsdale D, Li M (2004) NNC 55-0396 [(1S, 2S)-2-(2-(N-(3-benzimidazol-2-yl) propyl)-N-methylamino)ethyl)-6-fluoro-1,2,3,4-tetrahydro-1-isopropyl-2-naphthyl cyclopropanecarboxylate dihydrochloride]: A new selective inhibitor of T-type calcium channels. *J. Pharmacol. Exp. Therapeutics* 309: 193–199.
- Huguenard JR, McCormick DA (1992) Simulation of the currents involved in rhythmic oscillations in thalamic relay neurons. *J. Neurophys.* 68: 1373–1383.
- Inoue T, Watanabe S, Kawahara S, Kirino Y (2000) Phase-dependent filtering of sensory information in the oscillatory olfactory center of a terrestrial mollusk. *J. Neurophysiol.* 84: 1112–1115.
- Inoue T, Inokuma Y, Watanabe S, Kirino Y (2004) In vitro study of odor-evoked behavior in a terrestrial mollusk. *J. Neurophysiol.* 91: 372–381.
- Jacklet JW, Tieman DG (2004) Nitric oxide and histamine induce neuronal excitability by blocking background currents in neuron MCC of *Aplysia*. *J. Neurophysiol.* 91: 656–665.
- Kawai F, Miyachi E (2001) Modulation by cGMP of the voltage-gated currents in newt olfactory receptor cells. *Neurosci Res.* 39: 327–337.
- Kimura T, Suzuki H, Kono E, Sekiguchi T (1998a) Mapping of interneurons that contribute to food aversion conditioning in the slug brain. *Learning & Memory* 4: 376–388.
- Kimura T, Toda S, Sekiguchi T, Kawahara S, Kirino Y (1998b) Optical recording analysis of olfactory response of the procerebral lobe in the slug brain. *Learning & Memory* 4: 289–400.
- Kimura T, Toda S, Sekiguchi T, Kirino Y (1998c) Behavioral modulation induced by food odor aversive conditioning and its influence on the olfactory responses of an oscillatory brain network in the slug *Limax marginatus*. *Learning & Memory* 4: 365–375.
- Kleinfeld D, Delaney KR, Fee MS, Flores JA, Tank DW, Gelperin A (1994) Dynamics of propagating waves in the olfactory network of a terrestrial mollusc: An electrical and optical study. *J. Neurophysiol.* 72: 1402–1419.
- Kopell N, Ermentrout GB (1986) Symmetry and phaselocking in chains of weakly coupled oscillators. *Comm Pure Appl. Math.* 39: 623–660.
- Korneev SA, Piper MR, Picot J, Phillips R, Korneeva EI, O'Shea M (1998) Molecular characterization of NOS in a mollusc: Expression in a giant modulatory neuron. *J. Neurobiol.* 35: 65–76.
- Korneev SA, Kemenes I, Straub V, Staras K, Korneeva EI, Kemenes G, Benjamin PR, O'Shea M. Suppression of nitric oxide (NO)-dependent behavior by double-stranded RNA-mediated silencing of a neuronal NO synthase gene. *J. Neurosci.* 22: RC227(1–5).
- Lam Y-W, Cohen LB, Wachowiak M, Zochowski MR (2000) Odors elicit three different oscillations in the turtle olfactory bulb. *J. Neurosci.* 20: 749–762.
- Largo C, Tombaugh GC, Aitken PG, Herreras O, Somjen GG (1997) Heptanol but not fluoroacetate prevents the propagation of spreading depression in rat hippocampal slices. *J. Neurophysiol.* 77: 9–16.
- Laurent G, Stopfer M, Friedrich RW, Rabinovich MI, Volkovskii A, Abarbanel HD (2001) Odor encoding as an active, dynamical process: Experiments, computation, and theory. *Annu. Rev. Neurosci.* 24: 263–297.
- Makings LR, Tsien RY (1994) Caged nitric oxide. *J. Biol. Chem.* 269: 6282–6285.
- Martin C, Gervais R, Hugues E, Messaoudi B, Ravel N (2004) Learning modulation of odor-induced oscillatory responses in the rat olfactory bulb: A correlate of odor recognition? *J. Neurosci.* 24: 389–397.
- Mills SL, Massey SC (2000) A series of biotinylated tracers distinguishes three types of gap junction in retina. *J. Neurosci.* 20: 8629–8636.
- Murakami M, Watanabe S, Inoue T, Kirino Y (2004) Odor-evoked responses in the olfactory center neurons in the terrestrial slug. *J. Neurobiol.* 58: 369–378.
- Murlis J, Willis MA, Carde RT (1990) Odour signals: Patterns in space and time. In: KB Doving, ed., *Proceedings of the Tenth International Symposium on Olfaction and Taste, Graphic Communication Systems, Oslo*, pp. 6–17.
- Murlis J, Elkinton JS, Carde RT (1992) Odor plumes and how insects use them. *Ann. Rev. Entomol.* 37: 505–532.
- Ozog MA, Siushansian R, Naus CC (2002) Blocked gap junctional coupling increases glutamate-induced neurotoxicity in neuron-astrocyte cocultures. *J. Neuropathol. Exp. Neurol.* 61: 132–141.
- Panchin Y, Kelmanson I, Matz M, Lukyanov K, Usman N, Lukyanov S (2000) A ubiquitous family of putative gap junction molecules. *Curr. Biol.* 10: R473–R474.
- Phelan P, Starich TA (2001) Innexins get into the gap. *Bioessays* 23: 388–396.

- Precht J, Cohen LB, Pesaran B, Mitra PP, Kleinfeld D (1997) Visual stimuli induce waves of electrical activity in turtle cortex. *Proc. Natl. Acad. Sci. USA* 94: 7621–7626.
- Precht JC, Bullock TH, Kleinfeld D (2000) Direct evidence for local oscillatory current sources and intracortical phase gradients in turtle visual cortex. *Proc. Natl. Acad. Sci. USA* 97: 877–882.
- Press WH, Teukolsky SA, Vetterling WT, Flannery BP (1999) *Numerical Recipes in C* (2nd ed.) Cambridge University Press, Cambridge, UK.
- Prior D, Gelperin A (1977) Autoactive molluscan neuron: Reflex function and synaptic modulation during feeding in the terrestrial slug *Limax maximus*. *J. Comp. Physiol.* 114: 217–232.
- Sanchez-Alvarez M, Lean-Olea M, Talavera E, Pellicer F, Sanchez-Islas E, Martinez-Lorenzana G (1994) Distribution of NADPH-diaphorase in the perioesophageal ganglia of the snail, *Helix aspersa*. *Neurosci. Lett.* 169: 51–55.
- Simoes-de-Souza FM, Roque AC (2004) A biophysical model of vertebrate olfactory epithelium and bulb exhibiting gap junction dependent odor-evoked spatiotemporal patterns of activity. *BioSystems* 73:25–43.
- Skinner FK, Zhang L, Perez Velazquez JL, Carlen PL (1999) Bursting in inhibitory interneuronal networks: A role for gap-junctional coupling. *J. Neurophysiol.* 81: 1274–1283.
- Spray DC, White RL, Mazet F, Bennett MV (1985) Regulation of gap junctional conductance. *Am. J. Physiol.* 248: H753–764.
- Stopfer M, Bhagavan S, Smith BH, Laurent G (1997) Impaired odour discrimination on desynchronization of odour-encoding neural assemblies. *Nature* 390: 70–74.
- Teyke T, Gelperin A (1999) Olfactory oscillations augment odor discrimination not odor identification by *Limax* CNS. *Neuroreport* 10: 1061–1068.
- Toda S, Kawahara S, Kirino Y (2000) Image analysis of olfactory responses in the procerebrum of the terrestrial slug *Limax marginatus*. *J. Exp. Biol.* 203: 2895–2905.
- Traub RD, Miles R (1991) *Neuronal Networks of the Hippocampus*. Cambridge University Press, Cambridge, UK.
- Wang JW, Flores J, Gelperin A (1999) Physiological and morphological studies of olfactory interneurons in an oscillatory network. *Soc. Neurosci. Abstr.* 25: 126.
- Wang JW, Flores J, Gelperin A, Denk W (2001) Initiation and propagation of calcium-dependent action potentials in a coupled network of olfactory interneurons. *J. Neurophysiol.* 85: 977–985.
- Wang XJ, Rinzal J (1993) Spindle rhythmicity in the reticularis thalami nucleus: Synchronization among mutually inhibitory neurons. *Neurosci.* 53: 899–904.
- Watanabe S, Kawahara S, Kirino Y (1998) Morphological characterization of the bursting and nonbursting neurones in the olfactory centre of the terrestrial slug *Limax marginatus*. *J. Exp. Biol.* 201: 925–930.
- Watanabe S, Kawahara S, Kirino Y (1999) Glutamate induces Cl⁻ and K⁺ currents in the olfactory interneurons of a terrestrial slug. *J. Comp. Physiol. A* 184: 553–562.
- Watanabe S, Inoue T, Murakami M, Inokuma Y, Kawahara S, Kirino Y (2001) Modulation of oscillatory neural activities by cholinergic activation of interneurons in the olfactory center of a terrestrial slug. *Brain Res.* 896: 30–35.
- Watanabe S, Inoue T, Kirino Y (2003) Contribution of excitatory chloride conductance in the determination of the direction of traveling waves in an olfactory center. *J. Neurosci.* 23(7): 2932–2938.
- Wehr M, Laurent G (1996) Odor encoding by temporal sequences of firing in oscillating neural assemblies. *Nature* 384: 162–166.
- Wong WT, Sanes JR, Wong ROL (1998) Developmentally regulated spontaneous activity in the embryonic chick retina. *J. Neurosci.* 18: 8839–8852.
- Yunker AMR (2003) Modulation and pharmacology of low voltage-activated (“T-type”) calcium channels. *J. Bioenergetics Biomembranes.* 35: 577–598.
- Zakharov IS, Hayes NL, Ierusalimsky VN, Nowakowski RS, Balaban PM (1998) Postembryonic neurogenesis in the procerebrum of the terrestrial snail, *Helix lucorum*. *J. Neurobiol.* 35: 271–276.
- Zhang Y, Perez Velazquez JL, Tian GF, Wu C-W, Skinner FK, Carlen PL, Zhang L (1998) Slow oscillations (1 Hz) mediated by GABAergic interneuronal networks in rat hippocampus. *J. Neurosci.* 18: 9256–9268.